한국광물학회지 제 13 권 제 4 호 (2000)
J. Miner. Soc. Korea, 13, 196-204 (2000)

Characteristics of Hydrothermal Chlorite and Its Interstratification with 7-Å Phase in Rhyodacitic Tuff, Western Pusan, Korea

열수변질기원 녹니석과 이에 수반된 혼합층상 광물의 특징

Chang Oh Choo (추창오)* · Soo Jin Kim (김수진)**

*Department of Geology, Kyungpook National University, Taegu 702-701, Korea
(경북대학교 자연과학대학 지질학과, E-mail: choocco@hanmail.net)
**School of Earth and Environmental Sciences, Seoul National University, Seoul 151-742, Korea
(서울대학교 자연과학대학 지구환경과학부)

ABSTRACT : We present characteristics of hydrothermal chlorite and its interstratification with 7-Å mineral phase that occur in the propylitic alteration zone of the Bobae sericite deposit formed in rhyodacitic tuff. Chlorite is found as disseminated fine-grained aggregate or replacement materials of precursor minerals such as Fe-oxides and amphibole. Based on X-ray diffraction (XRD), all chlorites belong to IIb polytype and the (060) reflections averaging 1.53~1.54 Å indicate a trioctahedral structure. Chemical compositions of chlorite show that the Fe/(Fe+Mg) values are mostly in the range of 0.44~0.53, and cation deficiencies in octahedral sites range from 0.06 to 0.37. Under scanning electron microscope (SEM), chlorite occurs as well-crystallized aggregates and is subparallely stacked in interstices or between grain boundaries of associated minerals. transmission electron microscopic (TEM) images reveal that chlorite shows regular layers with 14-Å spacings, locally interstratified with 7-Å or 21-Å periodicities. The 21-Å periodicity corresponds to the sum of the d_{001} values of chlorite and 7-Å phase. The chlorite packet coexisting with 7-Å layers displays abundant defects such as edge dislocations and layer terminations. Selected-area electron diffraction (SAED) indicates that chlorite and 7-Å phase are randomly interstratified in the mixed-layer areas. We propose a lateral change of layers for the polymorphic transition of 7-Å phase to chlorite.

Keywords : chlorite, interstratification, SEM, TEM.

요약 : 유문암질 응회암의 열수변질에 의하여 형성된 보배견운모 광산의 프로필리틱 열수변질대에서 나타나는 녹니석은 7Å 광물과 혼합층상구조를 가진다. 녹니석은 산점상 또는 황철석, 철산화물, 각섬석과 같은 일차광물을 교대한다. X선 회절분석에 따르면, 녹니석은 IIb형, 삼팔면체 구조를 가지며, Fe/(Fe+Mg) 비는 0.44~0.53, 팔면체자리의 양이온 결핍은 0.06~0.37 범위를 보인다. 주사전자현미경하에서 녹니석은 결정도가 높으며, 수반된 광물입자들의 간극이나 경계부에서 거의 평행하게 쌓인 형태를 보인다. 투과전자현미경하에서 녹니석은 규칙적인 14Å 층으로 주로 구성되나 국부적으로 7Å 또는 21Å 주기를 나타낸다. 21Å 층은 저면간격 d_{001}이 녹니석과 7Å 층의 합에 해당된다. 7Å 층과 함께 나타나는 녹니석은 가장자리변위와 층의 절단과 같은 결함구조를 나타낸다. 혼합층상구조가 발달한 부분에서의 회절점은 녹니석과 7Å 층이 무작위로 혼합된 구조임를 보여준다. 7Å 층은 횡적전이과정을 통하여 점차 녹니석으로 변해가는 것으로 보인다.

주요어 : 녹니석, 혼합층상, 주사전자현미경, 투과전자현미경.

Introduction

Chlorite commonly occurs in various geological settings and is one of the important phyllosilicates formed in hydrothermally altered rocks and geothermal systems (Large, 1975; Cathelineau and Nieva, 1985; Parneix *et al.*, 1985; Martnez-Serrano and Dubois, 1998). In general, hydrothermal chlorite is ubiquitous in the weakly altered area such as propylitic alteration zone in many hydrothermal ore deposits (Lowell and Guilbert, 1970; Shikazono and Kawahata, 1987; Choo, 1996). However, the origin of hydrothermal chlorite is not well understood compared to other types occurring in metamorphic and sedimentary terrains. Chlorite formed in hydrothermal environments presents chemical and structural characteristics that are different from those in sedimentary and low-temperature metamorphic rocks (Martinez-Serrano and Dubois, 1998). Most authigenic chlorites show compositional variations with increasing temperature and octahedral occupancy (McDowell and Elders, 1983; Cathelineau, 1988). Since chlorite may be interstratified or intergrown with another phyllosilicates, the chemical composition obtained could not represent chlorite completely (Jiang *et al.*, 1994; Martinez-Serrano and Dubois, 1998). Therefore, there are still several problems in interpreting chemical data of chlorite.

Hydrothermal chlorite is frequently found in the Bobae sericite deposit located between western Pusan and southern Kimhae. Chlorite generally occurs in the propylitic alteration zone of the Bobae sericite deposit as fine-grained aggregates or replacement materials of precursor minerals such as pyrite, Fe-oxides, and amphibole (Choo, 1996). The main episode forming this sericite deposit marks ages ranging from 79.4±2.1 to 65.9±1.7 Ma (Park, personal communication; Moon and Moon, 1995), as reported by the K-Ar method performed on sericite samples collected from the phyllic zone. The Bobae sericite deposit is known to have formed by alteration of acidic tuff during the late stage of the evolution of the Bulguksa Granite (Kim *et al.*, 1991; Choo, 1996). Its formation process was influenced by mixing of magmatic fluids with meteoric water at low oxygen fugacity and at low SO_4^{2-}/H_2S (Moon and Moon, 1995). We present mineralogical characteristics of chlorite and interstratified layers occurring as a hydrothermal product in the sericite deposit, using XRD, electron microprobe analysis (EMPA), SEM, and TEM.

Analytical Methods

XRD analyses of all samples were carried out for identification of constituent minerals using a Rigaku Geigerflex RAD3-C with Ni-filtered CuK radiation. Samples were analyzed on powdered and oriented mounts at 40 kV/30 mA in continuous and step scan modes. Optical microscope, SEM, backscattered electron (BSE) image and elemental X-ray analyses characterized the morphology and texture of associated minerals. Compositional analyses were performed on polished thin sections using a Cameca SX-50 automated electron microprobe. Wavelength dispersive spectrometry (WDS) analyses were made at accelerating voltage of 15 kV and probe current of 10 nA, with electron beam diameter of 5 μm. The structural formulae were calculated on the basis of 14 oxygens for chlorite. Mineralogical textures were observed by SEM and chemical analyses were made using energy dispersive spectrometry (EDS) using a JEOL JSM 840A scanning electron microscope. For TEM observations, the areas of interest were detached from thin sections and further thinned with an Ar ion miller until electron transparent edges were properly produced and then carbon coating was applied. Selected areas were investigated using Philips CM20 scanning transmission electron microscope operated at 200 kV with a side-entry stage. Selected area electron diffraction patterns were obtained, followed by the observation of 00*l* lattice fringe images.

Results

XRD Data

Fig. 1 shows a representative XRD pattern of chlorite, with quartz impurity (sample C20~30). Strong even-order reflections and weak odd-order reflections are revealed. Reflections are sharp, indicating that chlorite is well-crystallized. Relatively a strong (001) reflection at 14Å suggests that chlorite is not an Fe-rich variety. All chlorites analyzed for the present study belong to IIb polytype, which is evidenced by diagnostic reflections at 2.59, 2.53, 2.45, 2.39, and 2.23Å. The (060) reflections of the Bobae chlorite averaging 1.53~1.54Å indicate that chlorite has a trioctahedral structure. Solvation of ethylen-glycol caused no shift in the basal reflections, demonstrating that there is no interstratification in chlorite layers. In the previous XRD results on the Bobae sericitic deposit (Kim *et al.*, 1991; Moon and Moon, 1996), there are neither serpentine minerals nor interstratified minerals present, consistent with the present XRD data. However, conventional XRD technique may have limits in characterizing interstratification when very small amounts of serpentine layers or other phyllosilicates are interstratified with chlorite.

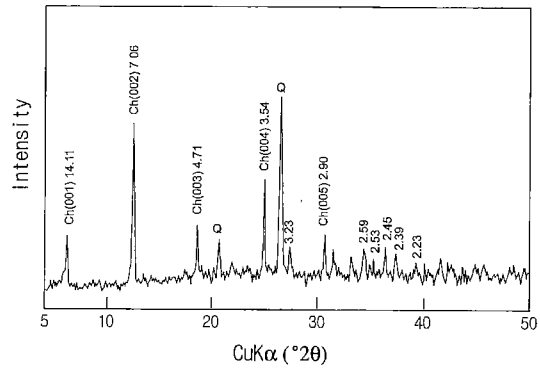

Fig. 1. XRD diffraction pattern of a powdered sample (C20-30) showing chlorite (Ch) and quartz (Q).

Electron Microprobe Analysis

Nomalized chlorite on the basis of 14 oxygens reveals that Al (VI) exceeds Al (IV) in all samples (Table 1), with Fe assumed to be ferrous. Chemical compositions of chlorite show that the Fe/(Fe+Mg) values are mostly in the range of 0.44~0.53, with the exception of one sample having 0.74 that occurs as a replacement of amphibole. Chemical compositions of most chlorites obtained by EMPA indicate that chlorite is not an Fe-rich phase, as also suggested by XRD data. From the present chemical data, the Fe/(Fe+Mg) ratio of the Bobae chlorite is intermediate. Cation deficiencies in octahedral sites range from 0.06 to 0.37. In general, the sum of interlayer cations including Ca, Na and K is inversely proportional to the octahderal occupancy. Fig. 2 shows average compositions of the Bobae chlorite and compares its chemistry with ideal end-member berthierine $(Fe_4Al_2)(Si_2Al_2)O_{10}(OH)_8$. Chemistry of most chlorites encompasses that of berthierine. The excess of Al (VI) over Al (IV) reflects vacancies in the octahedral sites, which is common in chlorite and berthierine (Brindley, 1982; Curtis *et al.*, 1985). Such an excess of Al (VI) may be related to the presence of intergrown other silicate minerals (Slack *et al.*, 1992). Several workers, using analytical TEM

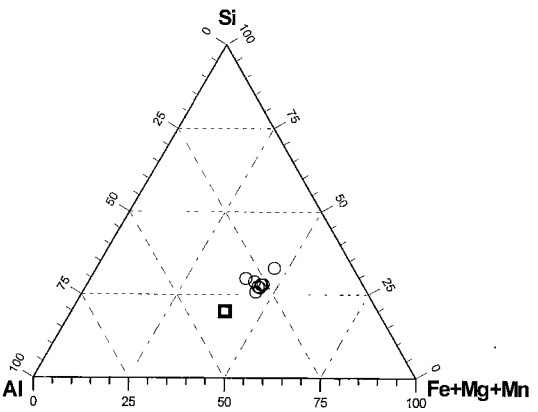

Fig. 2. Chemical compositions of chlorites plotted on a ternary diagram. Circles: bobae chlorites, square: ideal berthierine.

Table 1. Representative electron microprobe analyses of chlorite.

	K6	K13	B20-14	B20-15	C20-8	A9	B45	C2-93	C2-96
SiO_2	26.39	24.16	26.24	26.20	25.08	30.11	27.62	24.59	26.71
Al_2O_3	20.82	20.76	21.24	21.11	24.05	16.09	23.19	21.02	21.93
TiO_2	0.09	0.03	0.36	0.12	0.02	0.01	0.04	0.00	0.18
Cr_2O_3	0.08	0.11	0.09	0.02	0.04	0.08	0.02	0.01	0.00
FeO*	22.69	33.55	21.54	23.30	25.47	26.14	23.20	24.97	24.83
MgO	15.79	6.72	15.41	15.31	15.12	12.94	11.36	12.46	12.20
MnO	0.85	1.92	1.70	0.82	0.15	1.42	1.27	2.20	1.51
CaO	0.00	0.09	0.06	0.01	0.01	1.83	0.15	0.03	0.04
Na_2O	0.01	0.01	0.02	0.00	0.02	0.04	0.05	0.01	0.01
K_20	0.05	0.46	0.71	0.02	0.04	0.03	0.25	0.06	0.63
Total (wt.%)	86.77	87.81	87.37	86.91	90.00	88.69	87.15	85.35	88.04
	Structural formulae on the basis of 14 oxygens								
Si	2.78	2.70	2.75	2.76	2.57	3.17	2.88	2.69	2.81
Al(IV)	1.22	1.30	1.25	1.24	1.43	0.83	1.12	1.31	1.19
Sum(T)	4.00	4.00	4.00	4.00	4.00	4.00	4.00	4.00	4.00
Al(VI)	1.36	1.43	1.37	1.38	1.47	1.16	1.74	1.41	1.53
Ti	0.01	0.00	0.03	0.01	0.00	0.00	0.00	0.00	0.01
Cr	0.01	0.01	0.01	0.00	0.00	0.01	0.00	0.00	0.00
Fe	2.00	3.13	1.89	2.05	2.18	2.30	2.03	2.29	2.18
Mg	2.48	1.12	2.41	2.40	2.31	2.03	1.77	2.04	1.91
Mn	0.08	0.18	0.15	0.07	0.01	0.13	0.11	0.20	0.13
Sum(O)	5.94	5.87	5.86	5.91	5.97	5.63	5.65	5.94	5.76
Ca	0.00	0.01	0.01	0.00	0.00	0.21	0.02	0.00	0.00
Na	0.00	0.00	0.00	0.00	0.00	0.01	0.01	0.00	0.00
K	0.01	0.07	0.10	0.00	0.00	0.00	0.03	0.01	0.08
Sum(I)	0.01	0.08	0.11	0.00	0.00	0.21	0.06	0.01	0.08
Vacancy(O)	0.06	0.13	0.14	0.09	0.03	0.37	0.35	0.06	0.24
Fe/(Fe+Mg)	0.45	0.74	0.44	0.46	0.49	0.53	0.53	0.53	0.53

*Total Fe as ferrous

analysis or SEM/EDX coupled with XRD analysis, reported that there are no compositional variations between the coexisting chlorite and berthierine layers or serpentine mineral (Lee *et al.*, 1984; Jahren and Aagaard, 1989; Jiang *et al.*, 1992; Slack *et al.*, 1992; Abad-Ortega and Mieto, 1995; Ryan and Reynolds Jr., 1997)

Scanning Electron Microscopy

Chlorite occurs as well-crystallized aggregates under SEM image and is subparallely stacked in interstices or between grain boundaries (Fig. 3). Pyrite surrounded by chlorite is intensively altered. BSE images of chlorite formed in association with hematite are shown in Figs. 4a and b.

In the altered part of hematite crystals, chlorite is seen to occur together with quartz.

Fig. 3. Scanning electron micrographs of chlorite in sample C1-3 showing well-crystallized chlorite (C) around pyrite (PY) and quartz (Q).

Chlorite forms along the cracks or dissolved

cavities of hematite. Quartz crystal occurring in the inner core of the altered hematite is subsequently surrounded by chlorite and shows irregular grain boundaries due to alteration. X-maps show that there is slight variation in concentrations of Mg and Fe elements within the chlorite crystals (Figs. 4c and 4d)

Transmission Electron Microscopy

Chlorite exhibits complex features when observed under TEM. TEM lattice fringe images of chlorite commonly show straight, coherent layers with 14-Å layer. However, interstratificaiton of chlorite and 7-Å layers are also revealed. Electron diffraction patterns demonstrate that continuous streaking along the c-axis results from randomly interstratification of two different minerals. The lattice fringe images and electron diffraction patterns characteristic of chlorite and 7-Å layer are readily obtained, regardless of varying instrumental conditions during TEM observations. Therefore, we would like to regard the 7-Å layer interstratified with chlorite as 7-Å serpentine or berthierine, in spite of the absence of analytical TEM data on phyllosilicates in the present study. Fig. 5 shows locally curved-layers, numerous layer termina-

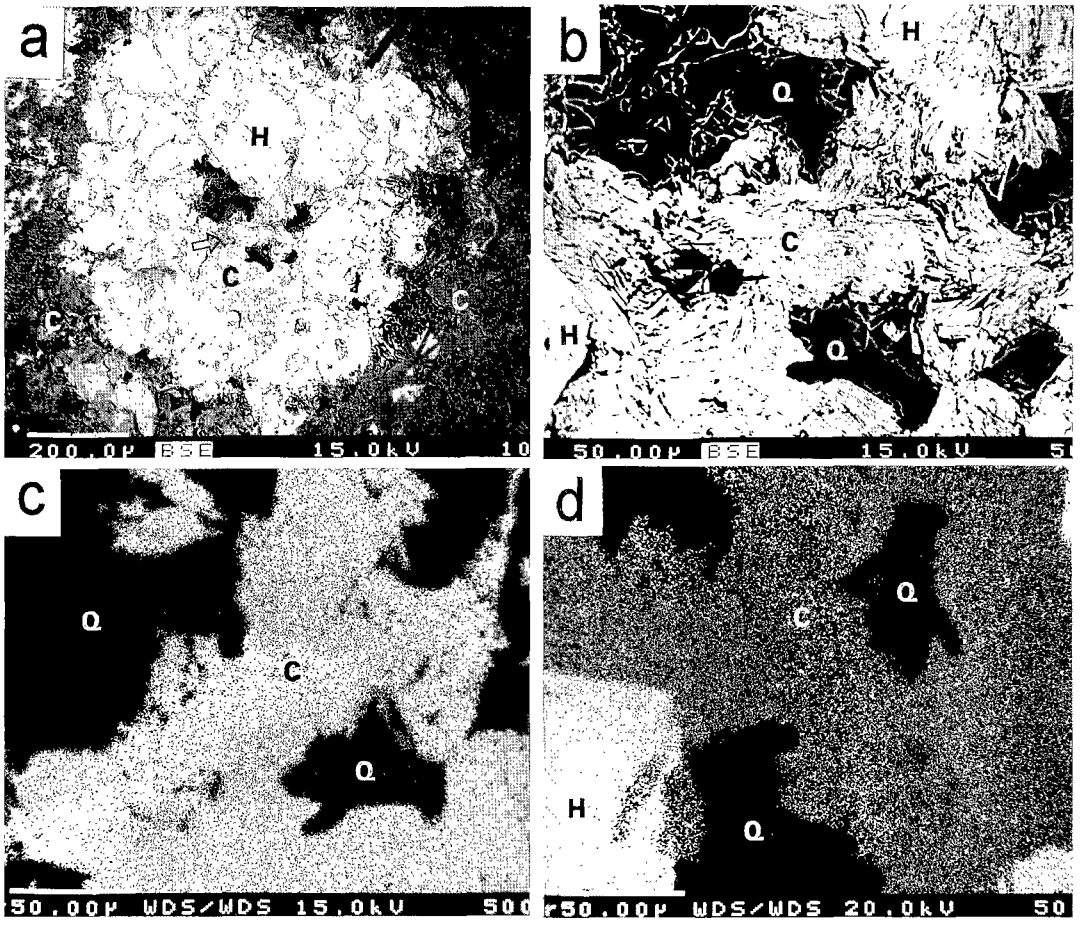

Fig. 4. Backscattered electron images of chlorite and X-ray maps in sample B4. (a) BSE image of chlorite (C), hematite (H) and quartz (Q). (b) Enlarged image of the arrowed area of (a). (c) X-ray map of Mg. (d) X-ray map of Fe.

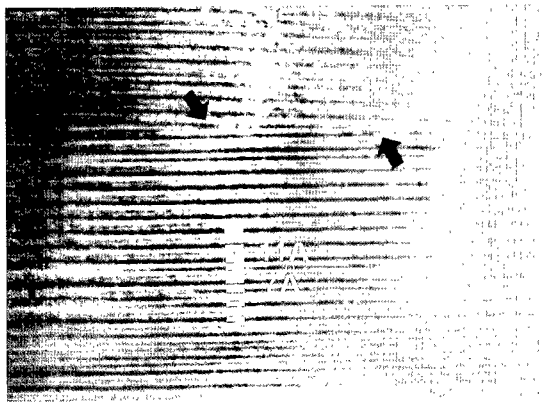

Fig. 5. TEM lattice fringe image of chlorite showing layer terminations (marked by arrows) and interstratification of 14-Å and 7-Å layers in chlorite packets.

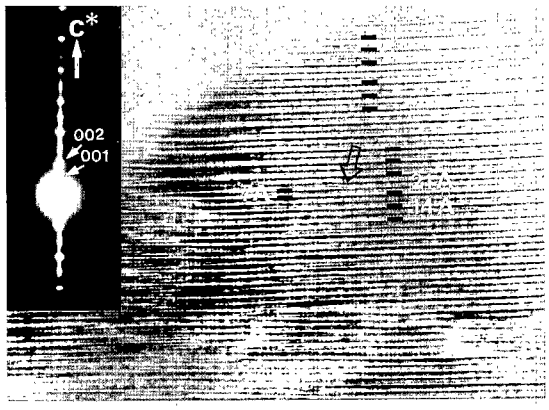

Fig. 6. TEM lattice fringe image of chlorite shows 14-Å, 7-Å, and 21-Å layers in chlorite packets. Layer terminations and dislocations are common. SAED pattern shows weak, diffuse odd-order reflections and strong, sharp even-order reflections along c* axis, respectively.

tions, and low angle grain boundaries.

TEM images of chlorite show regular layers with 14Å, locally interstratified with local 7-Å or 21-Å periodicities (Fig. 6). In such cases, 14-Å, 7-Å, and 21-Å periodicities, in order of abundance, are commonly observed. The 21-Å periodicity indicated by TEM images corresponds to the sum of the d_{001} values of chlorite (14Å) and 7-Å phase. Selected-area electron diffraction (SAED) pattern of the mixed-layer chlorite and 7-Å phase shows relatively weak, diffuse odd-order 00 *l* reflections and strong, sharp even-order 00 *l* reflections, respectively. The continuous streak along c* reveals that chlorite and 7-Å layers are randomly interstratified in the mixed-layer areas. There are no alternating packets of chlorite and 7-Å layers that are parallel or related by low-angle boundaries. Instead, individual 7-Å layers are present within the chlorite packet, and discontinuities between 14-Å and 7-Å layers are present in the mixed-layer area. Misfit dislocations in chlorite crystals are commonly observed (Fig. 7). In this case, the corresponding SAED pattern demonstrates different orientations of layers in the same unit and diffuseness along c* due to different layerings in chlorite packets. Wavy or modulated layers are observed within a single packet or between different packets (Fig. 8), which is possibly due to strains caused by misfits of layers.

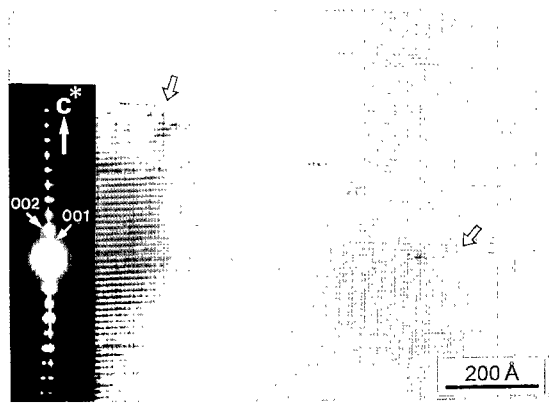

Fig. 7. TEM lattice fringe image shows layer terminations (marked by arrows) and misfits of layers. SAED pattern displays diffuse spots along c due to different orientation of layers.

Discussion

Until recently, interstratification of chorite-serpentine has attracted much attention because of the importance of the transition mechanism in phyllosillcates at low temperatures (Banfield *et al.*, 1994, 1995; Banfield and Bailey, 1996;

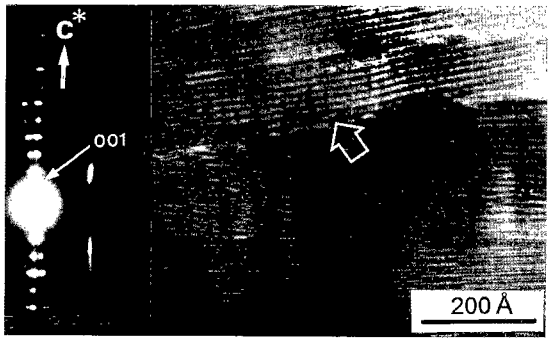

Fig. 8. Wavy or modulated layers are common (marked by arrows) between different packets. SAED pattern shows diffuse reflections due to different orientation of layers.

Xu and Veblen, 1996). Although there are some difficulties encountered in identifying such assemblage (Ahn *et al.*, 1988; Hillier and Velde, 1992; Abad-Ortega and Mieto, 1995), interstratification of chlorite and 7-Å phase has been clearly recognized in the present study. Temperature is still the most important variables influencing the transformation of phyllosilicates (Walker, 1993). For instance, the 7-Å phase always preceded the formation of chlorite in experimental studies of synthetic chlorites (Nelson and Roy, 1958; Velde, 1973). Ahn and Peacor (1985) proposed that a polymorphic transition from the 7-Å to the 14-Å phase occurs and the 7-Å phase forms as a precursor to the 14-Å phase metastably at low temperature. Requirements for interstratification include two end-member structure that are similar in the plane of intergrowth or nonequilibrium conditions which are common in low temperatures (Xu *et al.*, 1996). Walker and Thompson (1990) identified that the 7-Å and 14-Å interstratification occurs in the temperature range from 135~250℃ and the proportion of 7-Å phase decreases with increasing temperature. Interstratification of chlorite with 7-Å phase is found in the propylitic alteration zone of the Bobae sericite deposit, suggesting that the formation of 7-Å layers would be promoted at low temperatures. The chlorite geothermometer based on chemical composition (Cathelineau, 1985; Jiang *et al.*, 1994; Lu *et al.*, 1996) cannot be accepted as a generalized tool because there is some possibility that interstratification of chlorite with other phase occurs in the chlorite packet at the low temperature environment. It may require other physicochemical variables, as discussed by de Caritat *et al.* (1993), and should be used with caution, especially for hydrothermal system.

The facts that the 7-Å layers are always found in contact with 14-Å layers and no single discrete packet of the 7-Å layers exists suggest that 7-Å phase preceded the formation of chlorite. Because layers of chlorite and 7-Å phase are parallel or related by low-angle boundaries and layer terminations of 7-Å phase in the chlorite packet are common, the polymorphic transition of 7-Å phase to chlorite might be taken place through lateral change of layers. However, detailed investigations by the high resolution TEM are further needed.

At a first approximation, textural relations observed by SEM and TEM suggest that chlorite formed by replacement of Fe-bearing minerals, or precipitated directly from hydrothermal solutions having Fe component that might have been leached from precursor mafic minerals. Throughout the host rocks around the Bobae sericite deposit, propylitized rhyodacitific tuff underwent significant leaching of mafic components (Kim *et al.*, 1991; Choo, 1996). Hydrothermal alteration of silicate minerals might provide Si, Al, and Mg elements while pyrite and hematite supply Fe essential for chlorite or mixed-layer of chlorite and 7-Å phase. Interstratification of chlorite and 7-Å phase is detected by TEM, whereas only chlorite is identified by XRD patterns. Therefore, interstratification of chlorite and 7-Å phase is thought to be minimal in the propylitic alteration zone of the Bobae sericitic deposit.

Conclusions

The chlorite packet coexisting with 7-Å layers displays abundant defects such as edge dislocations and layer terminations in TEM

images. Chlorite shows regular 14-Å layers, locally interstratified with local 7-Å or 21-Å periodicities. Chlorite and 7-Å layers are randomly interstratified in the mixed-layer areas. Dislocations and modulated layers are possibly due to strains caused by misfits of layers. Lateral change of layers is proposed for the polymorphic transition of 7-Å phase to chlorite. Conventional XRD technique may have limit in characterizing interstratification when small amounts of 7-Å layers are interstratified with chlorite.

Acknowledgments

We are grateful to Professors J.H. Ahn, H.G. Cho and G.Y. Jeong for critical reviews and helpful comments on the manuscript.

References

Abad-Ortega, M. M. and Mieto, F. (1995) Genetic and chemical relationships between berthierine, chlorite and cordierite in nodules associated to granitic pegmatites of Sierra Albarraba (Iberian Massif, Spain). Contrib. Miner. Petrol., 120, 327-336

Ahn, J. H. and Peacor, D. R. (1985) Transmission electron microscopic study of diagenetic chlorite in Gulf Coast argillaceous sediments. Clays Clay Miner., 33, 228-236.

Ahn, J. H., Peacor, D. R., and Coombs, D. S. (1988) Formation mechanism of illite, chlorite and mixed-layer illite-chlorite in Triassic volcanogenic sediments from the Southland Syncline, New Zealand. Contrib. Miner. Petrol., 99, 82-89.

Banfield, J. F. and Bailey, S. W. (1996) Formation of regularly interstratified serpentine-chlorite minerals by tetrahedral inversion in long-period serpentine poytypes. Amer. Miner., 81, 79-91.

Banfield, J. F., Bailey, S. W., and Barker, W. W. (1994) Polysomatism, polytypism, defect structures, and reaction mechanisms in regularly and randomly interstratified serpentine and chlorite. Contrib. Miner. Petrol., 117, 137-150.

Banfield, J. F., Bailey, S. W., Barker, W. W., and Smith, II R. C. (1995) Complex polytypism: Relationships between serpentine structural characteristics and deformation. Amer. Miner., 80, 1116-1131.

Brindley, G. W. (1982) Chemical compositions of berthierines a review. Clays Clay Miner., 30, 153-155.

Choo, C. O. (1996) Mineralogy and genesis of napseok (sericite, pyrophyllite, dickite) in the Kimhae area, Korea. Ph.D. Thesis, Seoul National Univ., 196 p.

Cathelineau, M. (1988) Cation site occupancy in chlorites and illites as a function of temperature. Clay Miner., 23, 471-485.

Cathelineau, M. and Nieva, D. (1985) A chlorite solid solution geothermometer. The Los Azufres (Mexico) goethermal system. Contrib. Miner. Petrol., 91, 235-244.

Curtis, C. D., Hughes, C. R., Whiteman, J. A., and Whittle, C. K. (1985) Compositional variation within some sedimentary chlorites and some comments on their origin. Miner. Mag., 49, 375-386.

De Caritat P., Hutcheon I., and Walshe, J. L. (1993) Chlorite geothermometry: A review. Clays Clay Miner., 41, 219-239.

Hillier, S. and Velde, B. (1992) Chlorite interstratified with a 7- mineral: an example from offshore Norway and possible implications for the interpretation of the composition of diagenetic chlorites. Clay Miner., 27, 475-486.

Jahren, J. S. and Aagaard, P. (1989) Compositional variations in diagenetic chlorites and illites, and relationships with formation-water chemistry. Clay Miner., 24, 157-170.

Jiang, W. T., Peacor, D. R., and Slack, J. F. (1992) Microstructures, mixed layering, and polysomatism of chlorite and prograde berthierine in the Kidd Creek massive sulfide deposit, Ontario. Clays Clay Miner., 40, 501-514.

Jiang, W. T., Peacor, D. R., and Buseck, P. R. (1994) Chlorite geothermometry? contamination and apparent octahedral vacancies. Clays Clay Miner., 42, 593-605.

Kim, S. J., Choo, C. O., Park, H. I., and Noh, J. H. (1991) Mineralogy and genesis of hydrothermal deposits in the southeastern part of the Korean peninsula. Jour. Miner. Soc. Korea, 4, 129-140.

Large, R. R. (1975) Zonation of hydrothermal minerals at the Juno mine, Tennant Creek goldfield, central Australia. Econ. Geol., 70, 1387-1413.

Lee, J. H., Peacor, D. R., Lewis, D. D., and

Wintsch, R. P. (1984) Chlorite-illite/muscovite interlayered and interstratified crystals. A TEM/STEM study. Contrib. Miner. Petrol., 88. 372-385.

Lowell, J. D. and Guilbert, J. M. (1970) Lateral and vertical alteration-mineralization zoning in porphyry ore deposits. Econ. Geol., 65, 373-408.

Lu, J., Seccombe, P. K., and Walshe, J. L. (1996) Conditions of chlorite growth in the Hill End Goldfield, New South Wales, Australia: some predictions and evaluations. Can. Miner., 34, 9-21.

McDowell, S. D. and Elders, W. A. (1983). Allogenic layer silicate minerals in borehole Elmore #1, Salton Sea Geothermal Filed, California. Amer. Miner., 68, 1146-1159.

Martinez-Serrano, R. G. and Dubois, M. (1998) Chemical variations in chlorite at the Los Humeros geothermal system, Mexico. Clays Clay Miner., 46, 615-628.

Moon, J. W. and Moon, H. S. (1995) Occurrences and genetic environment of the Bobae sericite deposit, Pusan Area. Econ. Environ. Geol., 28, 93-107.

Moon, J. W. and Moon, H. S. (1996) Application of clay mineral geothermometry in the Bobae mine, Pusan, southeastern Korea. Econ. Environ. Geol., 29, 447-454.

Nelson, B. W. and Roy, R. (1958) Synthesis of the chlorites and their structural and chemical constitution. Amer. Miner., 43, 707-725.

Parneix, J. C., Beaufort, D., Dudoignon, P., and Meunier, A. (1985) Biotite chloritization process in hydrothermally altered granites. Chem. Geol., 51, 89-101.

Ryan, P. C. and Reynolds, R. C. Jr. (1997) The chemical composition of serpentine/chlorite in the Tuscaloosa Formation, United States Gulf Coast: EDX vs. XRD determinations, implications for mineralogic reactions and the origin of anatase. Clays Clay Miner., 45, 339-352.

Shikazono, N. and Kawahata, H. (1987) Compositional differences in chlorite from hydrothermally altered rocks and hydrothermal ore deposits. Can. Miner., 25, 465-475.

Slack, J. F, Jiang, W. T., Peacor, D. R., and Okita P. M. (1992) Hydrothermal and metamorphic berthierine from the Kidd Creek volcanogenic massive sulfide deposit, Timmins, Ontario. Can. Miner., 30, 1127-1142.

Velde, B. (1973) Phase equilibrium in the system MgO-Al_2O_3-SiO_2-H_2O: Chlorites and associated minerals. Miner. Mag., 39, 297-312.

Walker, J. R. (1993) Chlorite polytype geothermometry. Clays Clay Miner., 41, 260-267.

Walker, J. R. and Thompson, G. R. (1990) Structural variations in chlorite and illite in a diagenetic sequence from the Imperial Valley, California. Clays Clay Miner., 38, 315-321.

Xu, H. and Veblen, D. R. (1996) Interstratification and other reaction microstructures in the chlorite-berthierine series. Contrib. Miner. Petrol., 124, 291-301.

Xu, H., Zhang, Y., and Veblen, D. R. (1996) Periodic and nonperiodic interstratification in the chlorite-biotite series. Amer. Miner., 81, 1396-1404.

2000년 10월 2일 원고접수, 2000년 11월 24일 게재승인.